Section 7

Global and regional climate models, sensitivity and impact experiments, response to external forcing, monthly and seasonal forecasting.

Bayesian estimates of snow cover characteristics in Eurasia based on simulations with an ensemble of climate models

Arzhanov M.M.[1], Mokhov I.I.[1,2], Parfenova M.R.[1]
[1]*A.M. Obukhov Institute of Atmospheric Physics RAS*
[2]*Lomonosov Moscow State University*
arzhanov@ifaran.ru

The snow cover has a significant impact on the properties of the Earth's surface. A decrease in the albedo of the surface due to a decrease in the snow cover extent leads to an increase in the absorption of solar radiation with an intensification in the positive feedback. An analysis of the changes in the snow cover extent depending on the changes in the surface air temperature in the 21st century based on the simulations with models of global climate shows that the average estimates of the models' ensemble can be much smaller in absolute values than those obtained based on satellite observation data and by the models individually [1]. These results indicate the necessity of considering individual model features when using ensemble model estimates. Particularly, the Bayesian approach is applied to estimate the sensitivity of results to models choice by calculation of individual model weights and subsequent analysis of different variants of the weights [2].

This paper presents estimates of snow cover extent in Eurasia for 2000-2019 based on simulations with global climate models using a Bayesian approach compared to satellite observation data. The global climate models of the CMIP6 project (https://esgf-node.llnl.gov/projects/cmip6/)are used under the historical scenario are the following: (1) BCC-CSM2-MR, (2) CNRM-ESM2-1, (3) CanESM5, (4) FGOALS-f3-L, (5) IPSL-CM6A-LR, (6) MIROC6, (7) MPI-ESM1-2-LR, (8) MRI-ESM2-0, (9) NorESM2-LM. For each model, the weight was calculated based on the likelihood function by comparing it with the reference data - monthly average satellite data CDR (Climate Data Records) for the snow cover extent (https://climate.rutgers.edu/snowcover/) (Fig. 1).

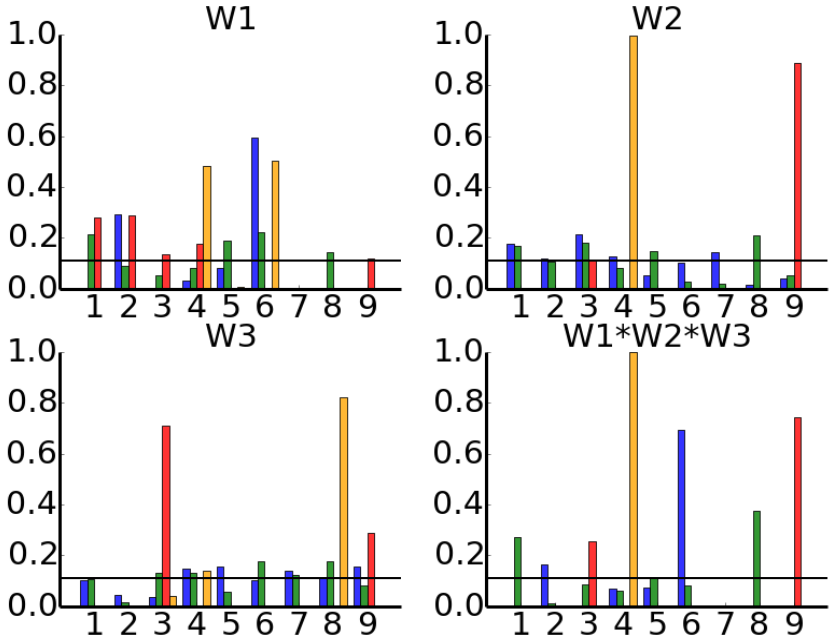

Figure 1. Normalized Bayesian weights for the models ensemble calculated for the snow cover extent in Eurasia in January (blue), April (green), July (red), and October (yellow) for the period 2000-2019. The horizontal line corresponds to the weights W0=1/N, where N=9 is the number of models in the ensemble.

To assess the quality of the models simulations results at different time scales, we calculate the weights for the long-term average (time scale corresponding to the length of the data series) (W1), the linear trend coefficient (interannual time scale) (W2), the standard deviation (interannual time scale) (W3) of the snow cover extent and their product (W4).

The largest intermodel variations are obtained for the summer and fall months for the weights W2 and W3. For winter and spring months, the distribution of weights W2 and W3 is more homogeneous compared to W1 and close to the value W0=1/N, where N=9 is the number of models in the ensemble. The estimates of the snow cover extent calculated with the weights W2 and W3 for the winter and fall seasons are close to the corresponding ensemble averages with the same weights W0 (Fig. 2).

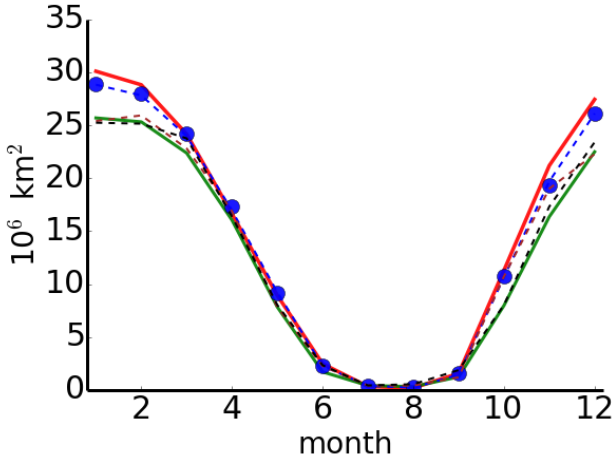

Figure 2. Snow cover extent in Eurasia over the period 2000-2019 based on ensemble of models with Bayesian weights (blue circles) and with W0 weights (green curve) compared to satellite observations (red curve). The dotted lines show the areas for the multiyear average (blue curve), trend (brown curve), and interannual variability (black curve) of the snow cover extent.

The results indicate that the application of the Bayesian approach significantly improves ensemble estimates of snow cover area, including the winter and fall seasons.

This work is supported by Russian Science Foundation project 19-17-00240.

References

[1] Parfenova M.R., Arzhanov M.M., Mokhov I.I. Projected changes in the snow cover extent in the 21st century in Eurasia according to simulations with the CMIP6 ensemble of climate models // Izv. Atmospheric and Oceanic Physics. 2022. Vol. 59. No. 3. P. 255-263.

[2] Parfenova M.R., Eliseev A.V., Mokhov I.I. Changes in the duration of navigation period in Arctic seas along the Northern Sea Route in the 21st century: Bayesian estimates based on calculations with the ensemble of climate models // Doklady Earth Sci. 2022. Vol. 507(1). P. 952-958.

Estimates of methane emissions from wet ecosystems of Western Siberia in the mid-Holocene and in the 21st century

M.M. Arzhanov
A.M. Obukhov Institute of Atmospheric Physics, RAS, Moscow, Russia
arzhanov@ifaran.ru

Observational data indicate a decrease in the area of wet ecosystems in Western Siberia due to the global warming, leading to thawing of permafrost and increased drainage [1]. Permafrost degradation also leads to the inclusion of thawed soil organic carbon into the global biogeochemical cycle. Changes in soil hydrology as well as soil temperature affect methane emissions from wet ecosystems. According to [2], global warming in 2000-2009 exceeded the Holocene optimum level. Regional changes in air temperature at high latitudes could be more significant. To estimate the methane emission from the wet ecosystems of Western Siberia, the main characteristics of the thermal regime of the soil for the mid-Holocene (around 6ka), the beginning (2000-2019) and the end (2080-2099) of the 21st century were calculated using a one-dimensional numerical scheme of heat transfer in the soil [3]. The scheme was forced by monthly air temperature and precipitation based on the global climate model ACCESS-ESM1-5 of the CMIP6 project (https: //esgf-node.llnl.gov/search/cmip6/) under scenarios midHolocene, historical and SSP5-8.5.

Fig. 1 shows the values of the average annual air temperature and the fraction of wet ecosystems in Western Siberia for the mid-Holocene, the beginning and end of the 21st century according to the ACCESS-ESM1-5 model. The regional air temperature at the beginning of the 21st century exceeds the mid-Holocene values. By the end of the 21st century, the air temperature is increasing, the negative average annual temperature persists only in the north of the region. A consistent decrease in the area of wet ecosystems has been revealed (fig. 1b).

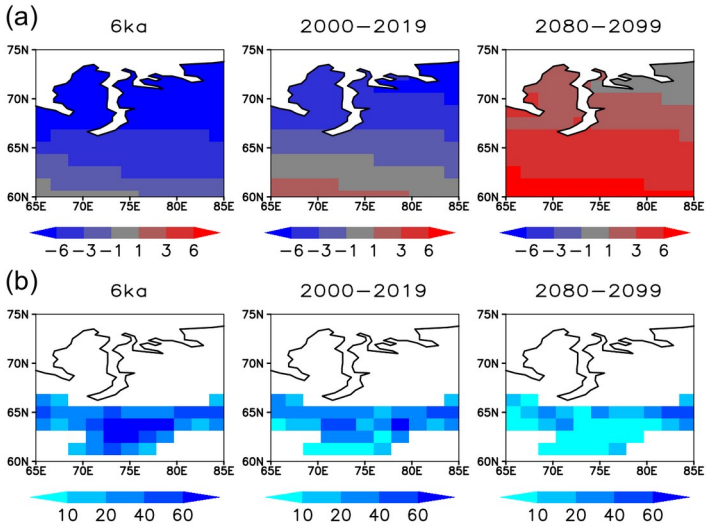

Fig. 1. a) Air temperature (ºC), b) Wetland fraction (%) according to calculations with the global climate model ACCESS-ESM1-5 for the mid-Holocene, the beginning and end of the 21st century.

According to the modeling results, at the beginning of the 21st century, the depth of seasonal thawing exceeded the values in the mid-Holocene (fig. 2a). By the end of the 21st century, the depth of seasonal thawing may exceed 2 m in the north of the region, and in the central and southern regions, seasonal thawing will change to seasonal freezing.

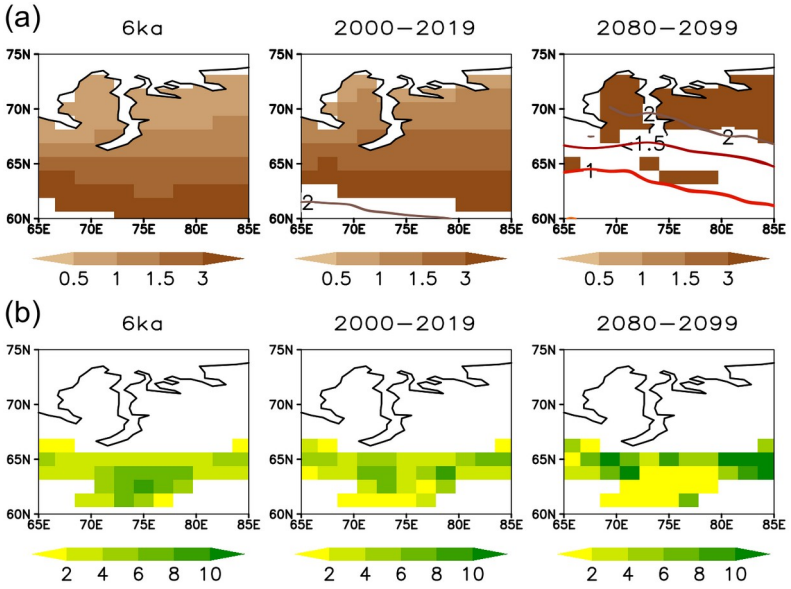

Fig. 2. a) Seasonal thaw (color fill) and frozen (isolines) depth (meters). b) Methane emissions ($gCH_4\ m^{-2}\ year^{-1}$) for the mid-Holocene, beginning and end of the 21st century.

Estimates of methane emissions in the south and in the central part of wetland are lower at the beginning of the 21st century compared to the mid-Holocene (fig. 2b). By the end of the 21st century, an increase in methane emission was revealed relative to the beginning of the 21st century and the mid-Holocene in the north and northeast of the wet ecosystems. The total methane emission from wet ecosystems of Western Siberia significantly increases in the 21st century (fig. 3).

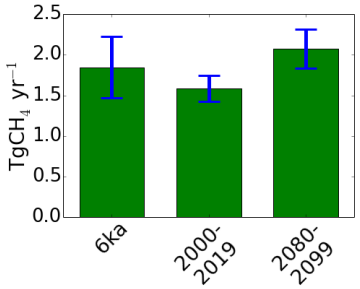

Fig. 3. Total methane emission ($TgCH_4\ year^{-1}$) from wet ecosystems of Western Siberia for the mid-Holocene, beginning and end of the 21st century.

The average values of methane emission at the end of the 21st century may exceed the values in the mid-Holocene, however, the interannual variability in the mid-Holocene is greater compared to the 21st century.

References

[1] Polishchuk YU.M., Kupriyanov M.A. Studying the dynamics of thermokarst lakes in the West Siberian Arctic based on the analysis of time series // Yugra State University Bulletin. 2022. Vol. 3(66). P. 37-144. doi: 10.18822/byusu202203137-144. (In Russian)

[2] Marcott S.A., Shakun J.D., Clark P.U., Mix A.C. Reconstruction of regional and global temperature for the past 11,300 years // Science. 2013. Vol. 339. P. 1198-1201.

[3] Arzhanov M.M., Denisov S.N., Mokhov I.I., Parfenova M.R. Estimates of natural methane emissions into the atmosphere in the regions of Western Siberia by model simulations // IOP Conf. Series: Earth and Environmental Science. 2022. N. 1040. doi: 10.1088/1755-1315/1040/1/012017.

Aerosol Indirect Effects in the UFS in Global Cloud Permitting Simulations

Anning Cheng[1], Fanglin Yang[2], and Shrinivas Moorthi[2]

[1.] Lynker@NOAA/NWS/NCEP/EMC, [2.] NOAA/NWS/NCEP/EMC

Introduction

Aerosols can impact the atmospheric energy budget directly by scattering, reflecting, and absorbing incoming solar radiation (aerosol direct effects, ADE). They can also indirectly influence weather and climate systems by acting as cloud condensation nuclei and/or ice nuclei, resulting in changes in cloud droplet number concentrations and sizes, modifying the microphysics, radiative properties, and even lifetime of clouds (aerosol indirect effects, AIE). The first indirect effects usually refer to the increase of droplet concentration and top of the atmosphere (TOA) albedo; the second involve changes of the microphysics, cloud life cycle, and surface precipitation, etc.

AIE are extensively studied in climate models by performing a control simulation with industrialized aerosol emissions and one with preindustrial emissions in order to study anthropogenic influences on climate. The indirect effects are mainly caused by sulfate related aerosols. The cloud radiation effect (CRE) from AIE (first and second) ranges from −1.1 to −3.7 W m^{-2} (Boucher et al. 2013). However, there are very few studies on the effects from turning on/off the whole aerosol indirect effects, the NonAll approach. In addition to the theoretical perspectives, the NoAll approach has more practical applications because most NWP models do not include any aerosol indirect effects. AIE on forecast skill is unknown.

In addition to factors such as poor understanding of physics and aerosol sources and sinks, model resolution is a major obstacle leading to uncertainties in modeling studies of AIE. Most models in the IPCC Intercomparison Studies have deep convection parameterization that does not include AIE. This study investigates AIE on cloud formation and the hydrometeorological cycle in UFS on a 3-km grid without parametrized deep convection and with a double-momentum microphysics scheme.

Experiment Design

The model used in this study is the atmosphere model of the NOAA Unified Forecast System (UFS), which has a 3 km horizontal resolution and 127 vertical levels extending to the mesopause (C3072L128 UFS). The Thompson microphysics, a double moment microphysics scheme, and the Rapid Radiation Transfer Model for GCM (RRTMG) are included in the physics package. MERRA2 (Modern-Era Retrospective analysis for Research and Applications, Version 2) aerosol climatology is used to drive the RRTMG radiation and activate the activation of ice nuclei (IN) or cloud condensation nuclei (CCN) of the microphysics scheme.

Four experiments were carried out with the same 2019100100 initial conditions and were run for 15 days 1) at 3-km resolution, no aerosol-cloud interaction, without parameterized deep convection (EXP ctl). The activation of IN/CCN in the microphysics scheme depends only on temperature. Therefore, only aerosol direct effect on radiation is activated in this experiment. 2) Same as (1) except the number concentrations of water friendly aerosol (NWFA) and ice-friendly aerosol (NIFA) are diagnosed from the Eidhammer-Thompson approach to activate IN/CCN using MERRA2 aerosol climatology (EXP aero). To investigate the effects of resolution, two more experiments at low resolution were performed: 3) same as (1) but using C768L127 with parameterized deep convection (13 km grid size, EXP ctl_low), and 4) same as (2) but using C768L127 and turning on deep convection (EXP aero_low).

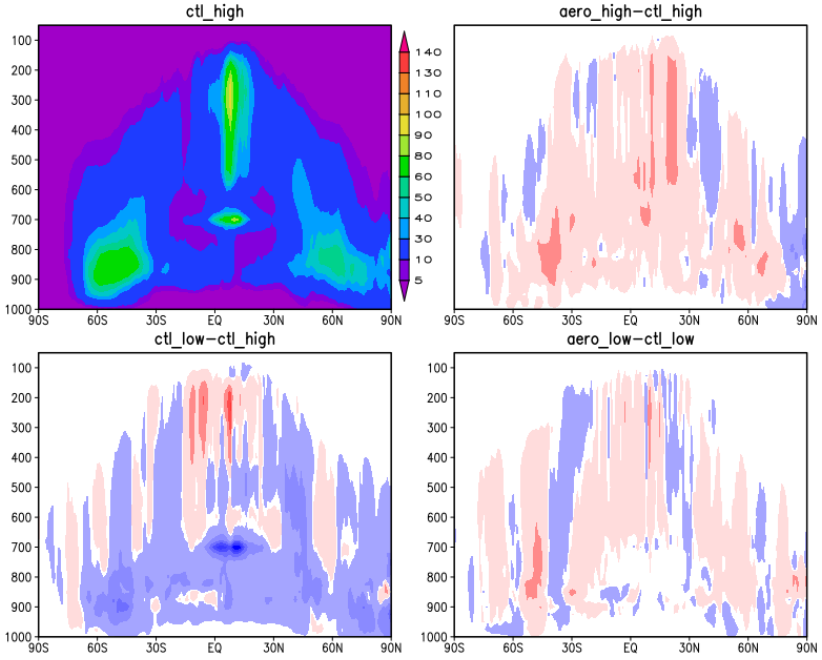

Figure 1. Vertical cross section of cloud liquid, cloud ice, and snow for the last 10 day mean from EXP ctl (a), diffrence between ctl and aero (b), EXP ctl_low (c), and the difference between aero_low and ctl_low (d)

Results

Aerosols provide more cloud condensation nuclei, so the cloud droplet number concentrations increase and cloud droplet sizes decrease (Twomey, 1974). This usually leads to more cloud liquid and ice in the atmosphere. This effect can be readily seen in Figure 1, which shows that the total cloud liquid, cloud ice, and snow are larger overall than in the control runs. This is more obvious in the cloud permitting runs in the Northern Hemisphere low latitudes and high troposphere. Note that the Thompson microphysics tends to treat ice as snow and this is one reason why snow is included. The coarse resolution runs tend to produce less hydrometers than the cloud permitting runs, especially for the low troposphere

(Figure 1c). Clouds with smaller particles and larger number concentrations should have higher albedo, and more TOA upward shortwave fluxes. The AIE effects represented by TOA upward SW differences between the control and aerosol is about -3.11 W m-2 and -0.65 W m-2 for the cloud permitting run and the low resolution run, respectively. Both are within the uncertainty range of the IPCC report. Large upward SW can be seen in the highly industrialized Eurasia region, central and north Africa, and storm track regime where sea salt serves as a main aerosol source. The AIE from the low resolution run is much smaller, probably because there is no aerosol parameterization in the deep convective scheme. The TOA SW differences caused by the resolution is nearly -14.38 W m-2, overwhelming the AIE. The large negative TOA SW near ITCZ where deep convection is active from the low resolution run relative to the high-resolution (Figure 2c) implies that less cloud ice and cloud water are produced in the deep convective parameterization.

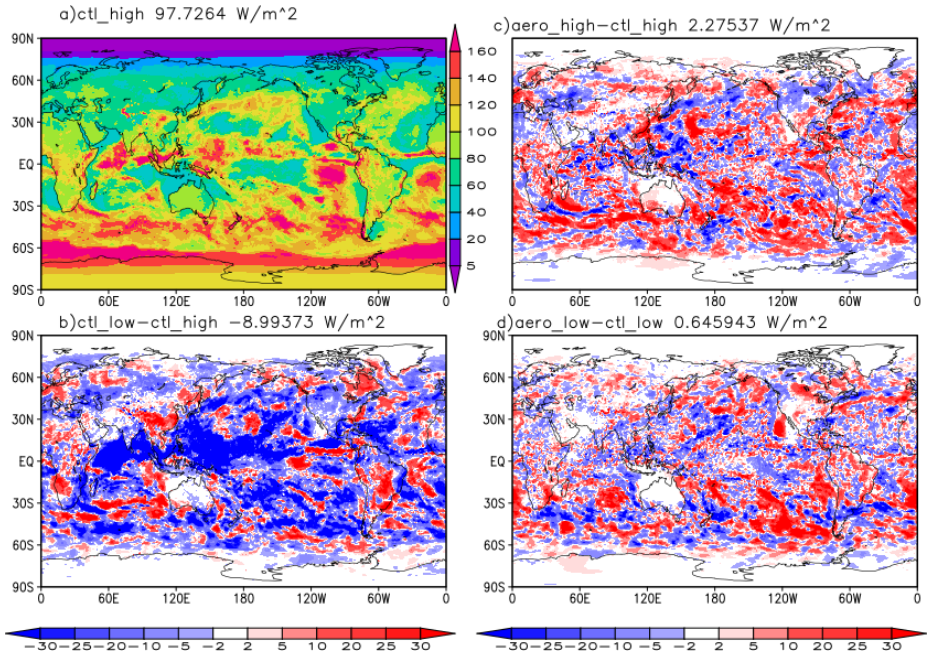

Figure 2. Same as Figure 1 except for mean global distribution of top of the atmosphere (TOA) upward shortwave radiation fluxes for the four experiments.

References

Boucher, O., D. Randall, P. Artaxo, C. Bretherton, G. Feingold, P. Forster, V.-M. Kerminen, Y. Kondo, H. Liao, U. Lohmann, P. Rasch, S.K. Satheesh, S. Sherwood, B. Stevens and X.Y. Zhang, 2013: Clouds and Aerosols. In: *Climate Change 2013: The Physical Science Basis. Contribution of Working Group I to the Fifth Assessment Report of the Intergovernmental Panel on Climate Change* [Stocker, T.F., D. Qin, G.-K. Plattner, M. Tignor, S.K. Allen, J. Boschung, A. Nauels, Y. Xia, V. Bex and P.M. Midgley (eds.)]. Cambridge University Press, Cambridge, United Kingdom and New York, NY, USA.

Twomey S (1974), Pollution and the planetary albedo. *Atmos. Environ.* 8, 1251–1256.

Characteristics of clouds in the Arctic Ocean:
Comparison of Arctic-CORDEX regional model's data with satellite observations

A V Chernokulsky[1], A I Narizhnaya[1], I I Mokhov[1], A. Rinke[2]

[1] *A.M. Obukhov Institute of Atmospheric Physics, Russian Academy of Sciences, Moscow, Russia*

[2] *Alfred Wegener Institute, Helmholtz Centre for Polar and Marine, Potsdam, Germany*

Introduction

Clouds play one of the key roles in the Arctic climate system by impacting on the regional energy budget and acting in several influential climate feedbacks. The Arctic cloud cover is sensitive to different climatic factors such as sea ice extent and atmospheric circulation indices. Climate and numerical weather prediction models, including regional models, simulate the Arctic cloud cover imperfectly, with non-negligible biases. The models may significantly benefit from inter-comparisons between the observed cloud cover and the corresponding quantities from historical model runs. It is of note, that for the Arctic-CORDEX regional model ensemble such intercomparison has not been performed previously for the entire Arctic.

Data and methods

This paper presents first results of comparative analysis of cloud characteristics, i.e., cloud liquid, ice and total water path (CLWP, CIWP and CTWP, respectively), that based on data from six regional models of the Arctic-CORDEX project. In particular, we used data from CCCma CanRCM4, DMI HIRHAM5, SMHI RCA4, SMHI RCA4–SN, ULg MAR3.6, and UQAM CRCM5-SN models. Model data were compared with the CERES satellite data (the SYN1deg_4.1 product). All data were bilinearly interpolated into the unified 0.25-degree grid cell.

Results

Comparison of cloud characteristics was carried out for different underlying surfaces (open water and sea ice). Distributions of cloud characteristics (Figure 1) and median values (Table 1) for all grid cells over open water and solid-ice regions were intercompared among models and satellite data for the mutual period from 2001 to 2010 for the cold portion of the

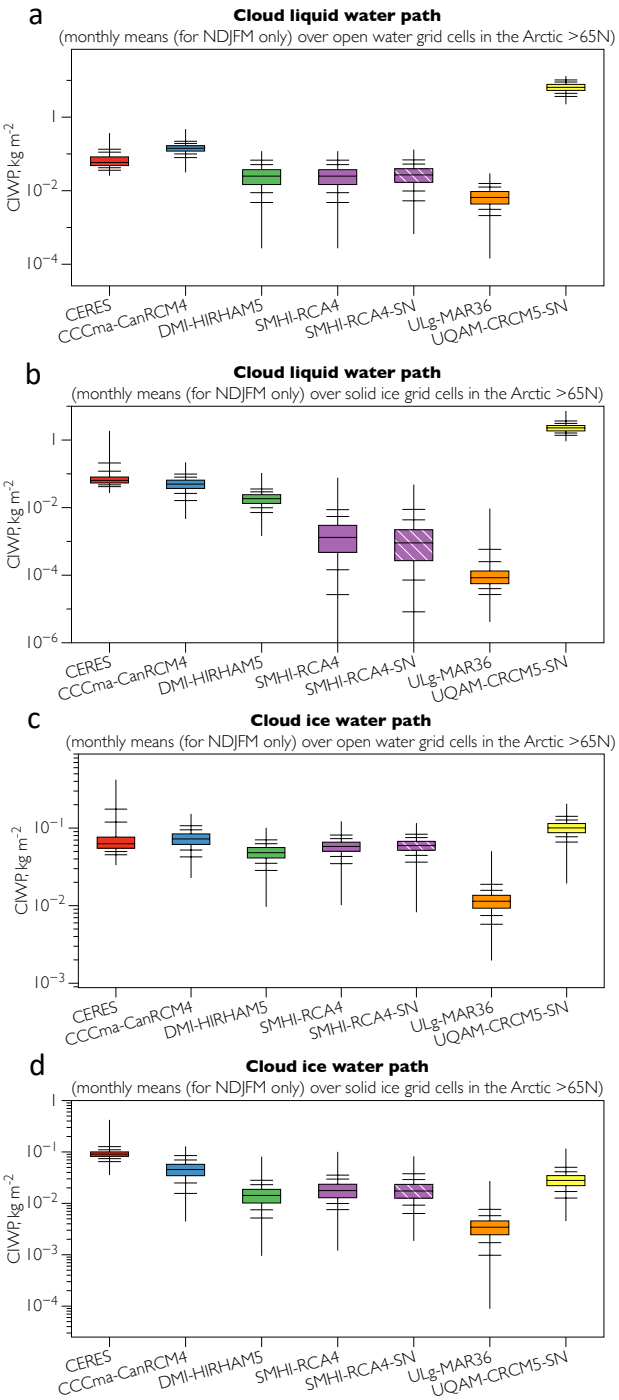

Figure 1. Box-plots for CLWP (a, b) and CIWP (c, d) over open-water (a, c) and solid-ice regions (b, d) for various data. Color boxes show interquartile range, while horizontal ticks stand for 2.5, 10, 90 and 97.5 percentiles.

Corresponding author: Alexander Chernokulsky, A.M. Obukhov Institute of Atmospheric Physics, Russian Academy of Sciences, Moscow, Russia.
E-mail: a.chernokulsky@ifaran.ru

year (months from November to March) for the Arctic Ocean (north of 65N).

Cloud characteristics	CLWP, kg m^2		CIWP, kg m^2		CTWP, kg m^2	
Underlying surface	Solid ice	Open water	Solid ice	Open water	Solid ice	Open water
models						
CCCma CanRCM4	0.050	0.142	0.046	0.072	0.095	0.217
DMI HIRHAM5	0.018	0.080	0.014	0.048	0.033	0.129
SMHI RCA4	0.001	0.025	0.018	0.058	0.019	0.083
SMHI RCA4–SN	0.001	0.027	0.017	0.059	0.018	0.088
ULg MAR3.6	0.001	0.007	0.003	0.011	0.004	0.018
UQAM CRCM5-SN	*2.288*	*6.457*	0.028	0.100	*2.317*	*6.558*
Observations						
CERES	0.064	0.058	0.091	0.063	0.155	0.121

Table 1. Median values of cloud characteristics for different regions of the Arctic Ocean in November-March. Suspicious values that should be checked are shown in italics.

In general, values of CIWP and CLWP among models vary substantially, especially those for CLWP with the revealed difference for several orders. We found better agreement between models and satellite observations for both CLWP and CIWP over open water and lower agreement over solid-ice regions. When comparing contribution of liquid and ice water path to CTWP, part of models shows higher values for CIWP (i.e., SMHI RCA4, SMHI RCA4-SN, ULg MAR3.6), while other models show the opposite. It is of note that data for CLWP (and for CTWP respectively) for UQAM CRCM5-SN model should be checked since it is suspiciously two order higher than the one for other datasets.

The CERES data displays higher values for CLWP than for CIWP (the ratio CIWP/CLWP is around 0.7 over solid-ice regions and around 0.92 over open-water regions). In general, CERES data display higher values of CTWP over solid-ice regions while models show the opposite.

It is of note that while models display a substantial difference for CLWP and CIWP values, they agree well in surface downward longwave radiation (Figure 2). Presumably, this should imply different relationship between cloud emissivity (that associated with cloud water path) and surface downward longwave radiation in each model. This finding has to be evaluated properly in future.

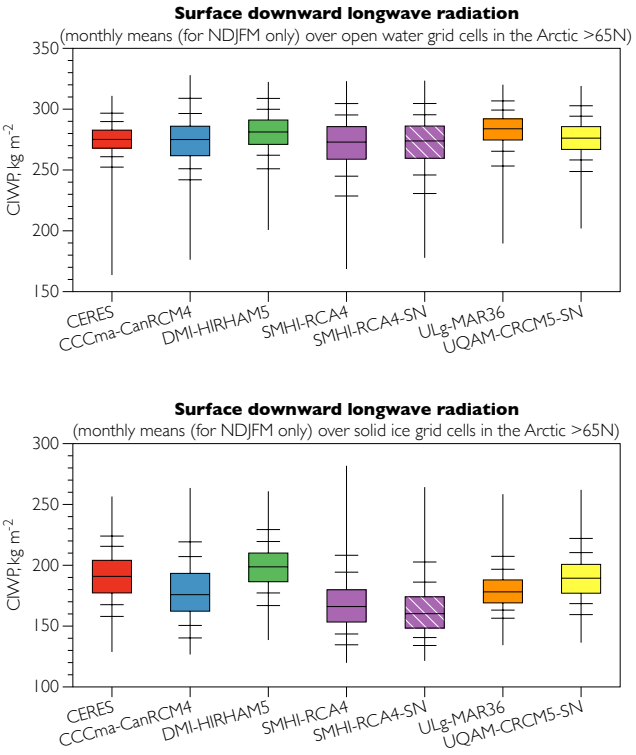

Figure 2. The same as for Figure 1 but for surface downward longwave radiation.

Model estimates of the process of complete permafrost degradation under warming in the region of the Yamal Peninsula

Malakhova V.V.[1], Mokhov I.I.[2,3], Arzhanov M.M.[2]

[1]Institute of Computational Mathematics and Mathematical Geophysics, Siberian Branch, Russian Academy of Sciences, Novosibirsk, 630090 Russia
[2]A.M. Obukhov Institute of Atmospheric Physics, Russian Academy of Sciences, Moscow, 119017 Russia
[3]Lomonosov Moscow State University, Moscow, 119991 Russia

The climate at high latitudes is characterized by great variability and sensitivity to natural and anthropogenic forcings, with rapid warming in recent decades. Particularly significant climatic changes occur in the cryolithozone during the permafrost degradation and the violation of the methane hydrates stability. Here, changes in the permafrost and methane hydrates stability zone (MHSZ) under conditions of future warming over a long period of time of 20 000 years in the region of the Yamal Peninsula from model simulations are presented.

To calculate the thermal state of the permafrost and thermobaric conditions of the existence of gas hydrates, the one-dimensional model of the thermophysical processes in soils was used [2,3]. The changes in the monthly mean surface temperature for the northern regions of Western Siberia were set as the upper boundary conditions for heat transfer in the soil. Changes in the permafrost and MHSZ over the last 130 000 years were estimated with the use the changed boundary conditions on the basis of the CLIMBER-2 global climate model simulations before 1850 [4,5]. The permafrost state and MHSZ for the Yamal Peninsula region from 1850 to 2300 were calculated numerically using the results of the CMIP6 ensemble of the climatic model simulations. The results of calculations of the surface temperature and precipitation with the CanESM5, IPSL-CM6A-LR, ACCESS-ESM1-5 and MRI-ESM2-0 climate models under “historical” and SSP5-8.5 scenarios for the 21st century with the ScenarioMIP long-term extention up to 2300 [1] were used (Fig. 1). In addition, permafrost and MHSZ were calculated for the next 20 000 years with the boundary conditions using climate model simulations with the boundary conditions fixed at the level of 2300 (temperature and precipitation, simulated under the SSP5-8.5 scenario until 2100 and ScenarioMIP CMIP6 for the period of 2100–2300) [5]. Different values of the heat flux from the Earth interior were used: 50 mW/m^2 and 75 mW/m^2.

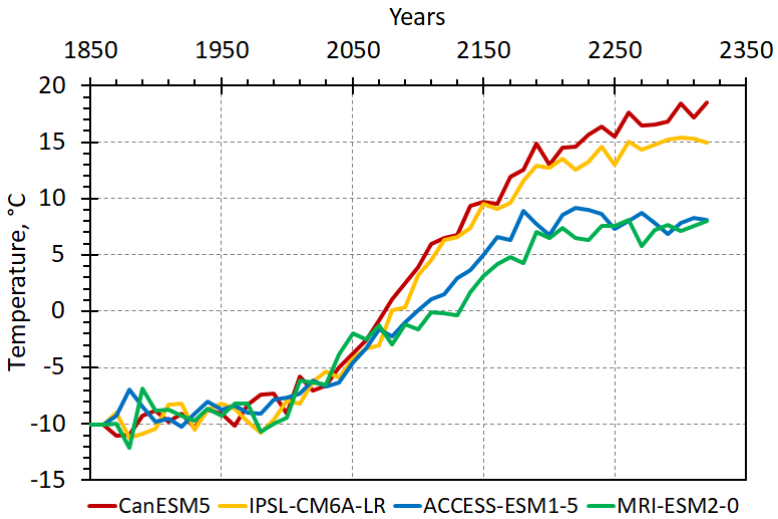

Figure 1. Changes in the annual mean surface temperature in the Yamal Peninsula region, used as the boundary conditions for the period of 1850–2300 according to the climate model simulations (CanESM5, IPSL-CM6A-LR, ACCESS-ESM1-5 and MRI-ESM2-0) under “historical” and SSP5-8.5 scenarios for the 21st century with the ScenarioMIP long-term extention up to 2300.

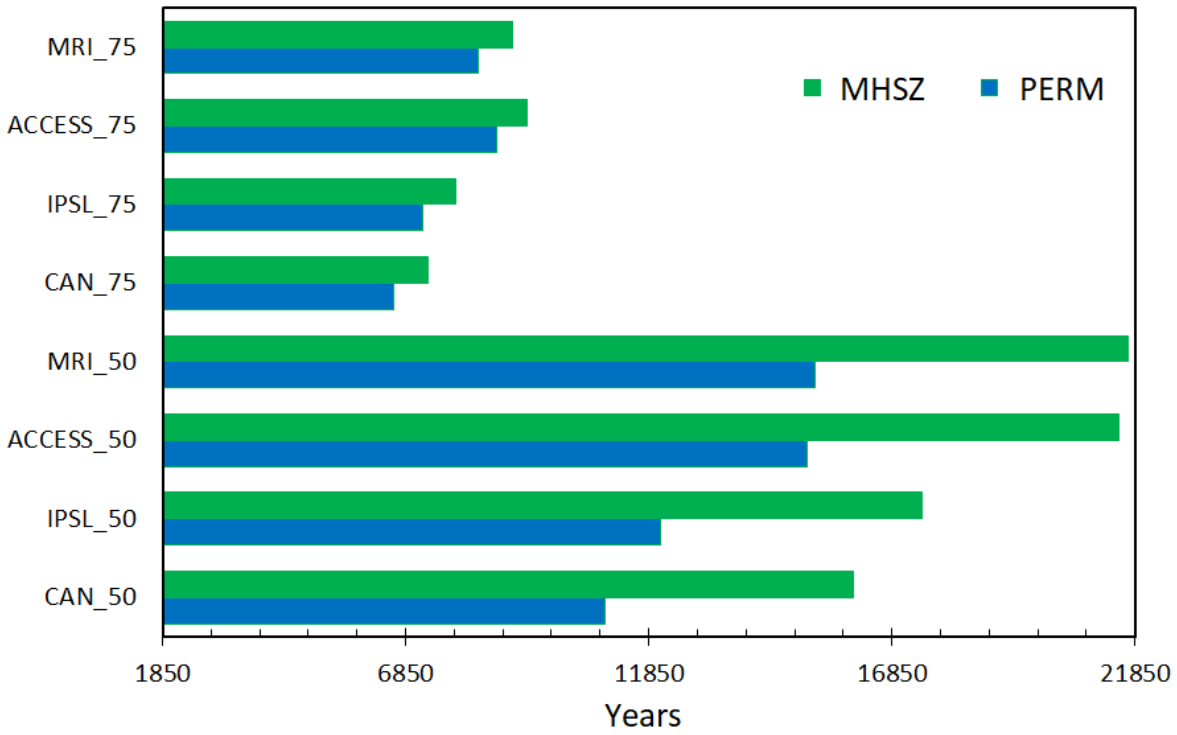

Figure 2. Time of the disappearance of permafrost (PERM) and of the methane hydrates stability zone (MHSZ) from model simulations with different geothermal heat flux: 50 mW/m^2 (CAN_50, IPSL_50, ACCESS_50 and MRI_50) and 75 mW/m^2 (CAN_75, IPSL_75, ACCESS_75 and MRI_75).

The estimates of the limiting conditions for the existence of permafrost at different depths and the conditions for the stability of methane hydrates were obtained. According to model simulations under historical" and SSP5-8.5 scenarios for the 21st century with the ScenarioMIP long-term extention up to 2300 the permafrost survives, at least, for 5 millennia after present conditions or even longer provided that heat flux 75 mW/m^2. For smaller geothermal flux (50 mW/m^2) the period of complete degradation of permafrost increases to 11-15 millennia, depending on the scenario (Fig. 2). According to simulations methane hydrate stability zone disappears not earlier that at 7300-9300 for the heat flux 75 mW/m^2. For smaller geothermal heat flux, 50 mW/m^2, the moment of complete disappearance of the MHSZ ranges from 16 to 21.7 millennia, depending on the forcing scenario (Fig. 2).

References

1. O'Neill D.C. et al. The Scenario Model Intercomparison Project (ScenarioMIP) for CMIP6. Geosci. Model. Dev., 2016, 9, 3461-3482.
2. Arzhanov M.M., Malakhova V.V., Mokhov I.I. Modeling thermal regime and evolution of the methane hydrate stability zone of the Yamal peninsula permafrost. Permafr. Periglac. Process, 2020, **31**, 487–496.
3. Gavrilov A., Malakhova V., Pizhankova E., Popova A. Permafrost and gas hydrate stability zone of the glacial part of the East-Siberian shelf. Geosci., 2020, **10**, 484, doi:10.3390/geosciences10120484.
4. Ganopolski A., Winkelmann R., Claussen M. Simulation of the last glacial cycle with a coupled climate ice-sheet model of intermediate complexity. Clim. Past, 2010, **6** (2), 229-244.
5. Mokhov I.I., Malakhova V.V., Arzhanov M.M. Model estimates of intra- and intersentennial degradation of permafrost on the Yamal Peninsula under warming. Doklady Earth Sci., 2022, **506** (2), 782–789. DOI: 10.1134/S1028334X22600426.

Atmospheric centers of action over oceans in the Southern Hemisphere: Possible changes in the 21st century from CMIP6 model simulations

Mokhov I.I.[1,2], Osipov A.M.[2], Chernokulsky A.V.[1]

[1]A.M. Obukhov Institute of Atmospheric Physics RAS
[2]Lomonosov Moscow State University
mokhov@ifaran.ru

An analysis of possible changes of the atmospheric centers of action (ACA) in the Southern Hemisphere under global warming was carried out. We used the results of simulations with climate models of the CMIP6 ensemble with the SSP5-8.5 scenario for the 21st century. The quality of the ACAs simulations was evaluated by comparison of the CMIP6 historical scenario with the ERA5 reanalysis data (https://www.ecmwf.int/en/forecasts/datasets/reanalysis-datasets/era5) for the base period 1981-2005.

The areas corresponding to each of the analyzed ACAs were identified similar to (Mokhov et al., 2020). Within the area corresponding to ACA, the mean sea level pressure Pc was determined with increased or decreased pressure for anticyclonic or cyclonic conditions, respectively (see also (Mokhov et al., 2018; Mokhov et al., 2021). The ACA intensity was characterized both by the pressure at sea level in the ACA region Pc and by the corresponding pressure drop Ic relative to the mean hemispheric pressure P_H at the sea level. We also analyzed the relative changes in the ACA intensity Ic = Ic/δIc - when normalizing Ic to the corresponding standard deviations (SD) δIc.

Two model ensembles were analyzed separately, i.e., all CMIP6 models that provide information on sea-level pressure (53 models and their versions), and selected models that best simulate both sea-level pressure field and intensity of ACAs (similar to (Mokhov et al., 2022)).

Table 1. Intensity Ic [hPa] of ACAs in the Southern Hemisphere for winter and summer from simulations with selected 11 CMIP6 ensemble of climate models (under the historical scenario) and by ERA5 reanalysis data for the base period 1981-2005. The standard deviations (SD) of the ACA intensity are given in parentheses. The corresponding estimates for the selected models are given in square brackets.

ACA Seasonal Mean Intensity (hPa)	Winter (JJA)		Summer (DJF)	
	Reanalysis	CMIP6 models	Reanalysis	CMIP6 models
South Pacific High	7.2 (±1.5)	8.5 (±1.6) [8.1 (±1.5)]	9.8 (±1.0)	9.6 (±0.9) [9.7 (±0.9)]
South Atlantic High	9.2 (±0.9)	11.4 (±1.0) [10.9 (±1.0)]	7.9 (±0.6)	8.3 (±0.7) [8.2 (±0.7)]
South Indian (Mascarene) High	11.3 (±1.2)	13.2 (±1.1) [13.0 (±1.0)]	8.7 (±0.7)	8.8 (±0.7) [8.7 (±0.7)]
South Pacific Low	-20.7 (±4.0)	-17.3 (±3.9) [-17.9 (±3.7)]	-18.3 (±2.8)	-17.6 (±2.7) [-17.5 (±2.6]
South Atlantic Low	-15.8 (±0.9)	-13.6 (±1.6)) [-14.3 (±1.6)]	-13.5 (±1.0)	-12.7 (±1.1) [-13.1 (±1.1)]
South Indian Low	-17.8 (±1.3)	-16.6 (±1.8) [-16.9 (±1.8)]	-12.4 (±1.1)	-12.0 (±1.1) [-12.3 (±1.1)]

Table 1 presents intensity Ic of ACAs over oceans in the Southern Hemisphere for winter and summer from simulations with CMIP6 ensemble of climate models and by ERA5 reanalysis data for the base period 1981-2005.

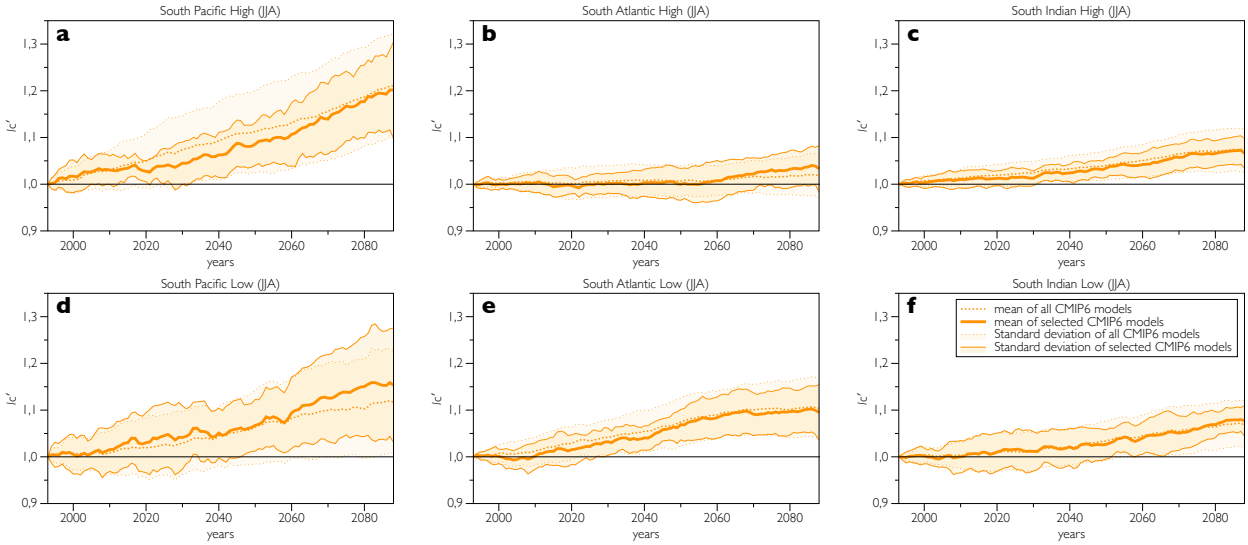

Figure 1. Changes in the winter (JJA) ACA intensity (normalized to SD for the base period 1981-2005) in the Southern Hemisphere from simulations with CMIP6 models under the SSP5-8.5 scenario. Here: (a) South Pacific High, (b) South Atlantic High, (c) South Indian (Mascarene) High, (d) South Pacific Low, (e) South Atlantic Low, (f) South Indian Low. SD ranges relative to 30-year moving averages are shaded, mean value for the ensemble is shown as well. Two ensembles are shown: the ensemble for the selected models is shown with solid lines, the ensemble with all CMIP6 models is shown with dashed lines (and paler shading),

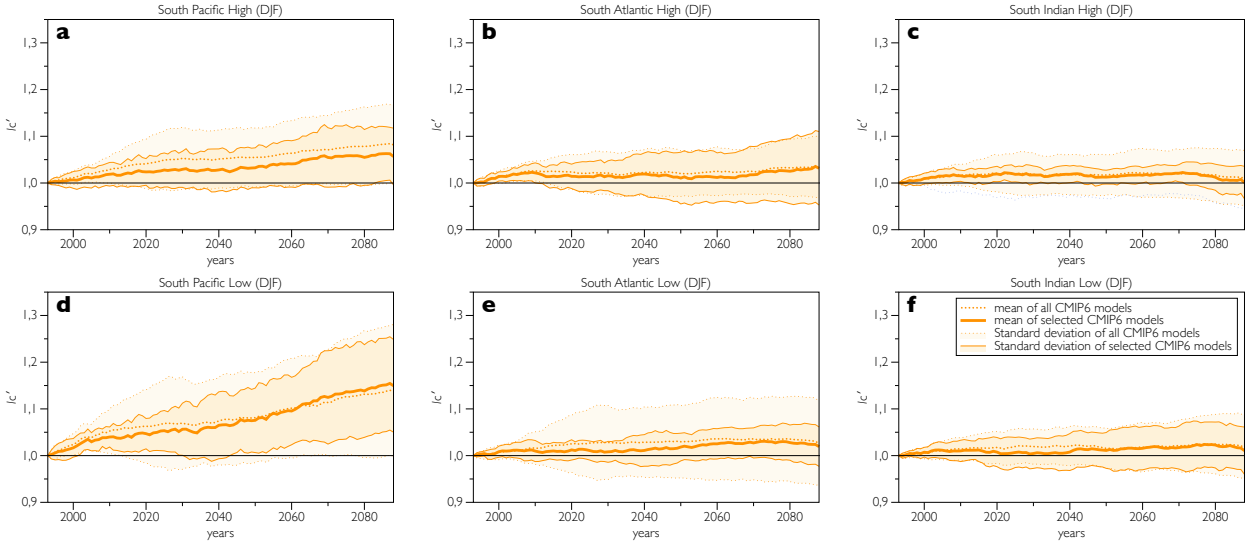

Figure 2. Same as Figure 1 but for changes in the summer (DJF).

According to ensemble simulations with CMIP6 models all analyzed ACAs over oceans in the Southern Hemisphere are intensified as a whole in the 21st century under scenario SSP5-8.5.

References

Mokhov I.I., Chernokulsky A.V., Osipov A.M. Changes in the characteristics of atmospheric centers of action. In: Intense Atmospheric Vortices and Their Dynamics. Ed. By I.I. Mokhov, M.V. Kurgansky, O.G. Chkhetiani. Moscow, GEOS, 2018, 398-403. (In Russian)

Mokhov I.I., Chernokulsky A.V., Osipov A.M. Atmospheric centers of action in the Northern and Southern Hemispheres: Features and variability. Rus. Meteorol. Hydrol., 2020, **45** (10), 749–761.

Mokhov I.I., Chernokulsky A.V., Osipov A.M. Atmospheric centers of action in the Northern and Southern Hemispheres: Tendencies of change in the 21st century from model simulations. Research Activities in Earth System Modelling, E. Astakhova (ed.), 2021, Rep. 51, 7, 11-12.

Mokhov I.I., Osipov A.M., Chernokulsky A.V. Atmospheric centers of action in the Northern Hemisphere: Current features and expected changes in the 21st century based on simulations with the CMIP5 and CMIP6 ensembles of climate models. Doklady Earth Sciences, 2022, **507** (2), 1132–1139.

Changes in coherence between different types of El-Nino

from observations and model simulations

Mokhov I.I.[1,2], Medvedev N.N.[2], Timazhev A.V.[1]

[1]A.M. Obukhov Institute of Atmospheric Physics RAS

[2]Lomonosov Moscow State University

mokhov@ifaran.ru

The strongest interannual variations in global surface temperature are associated with El Niño processes. Different types of El Niño phenomena are manifested, including the canonical El Niño event with the largest surface temperature anomalies in the equatorial latitudes of the Eastern Pacific Ocean and the so-called El Niño Modoki with the largest surface temperature anomalies (SST) in the central Pacific Ocean in the equatorial latitudes [1]. In this work, using cross-wavelet analysis [2], we estimate the features and changes in the relationship between different El Niño indices characterizing SST anomalies in the eastern (Nino3) and central (Nino4) equatorial regions of the Pacific Ocean (see also [3,4]), using observational data (https://psl.noaa.gov/gcos_wgsp/Timeseries/) and simulations with climate models of the CMIP6 ensemble (https://esgf-node.llnl.gov/projects/cmip6/).

Figures 1(a-d) show coherence of Nino3 and Nino4 anomalies for 1870–2020 by monthly data based on observations and from simulations with historical scenario with 3 climate models (ACCESS-CM2, CanESM5 and INM-CM5-0).

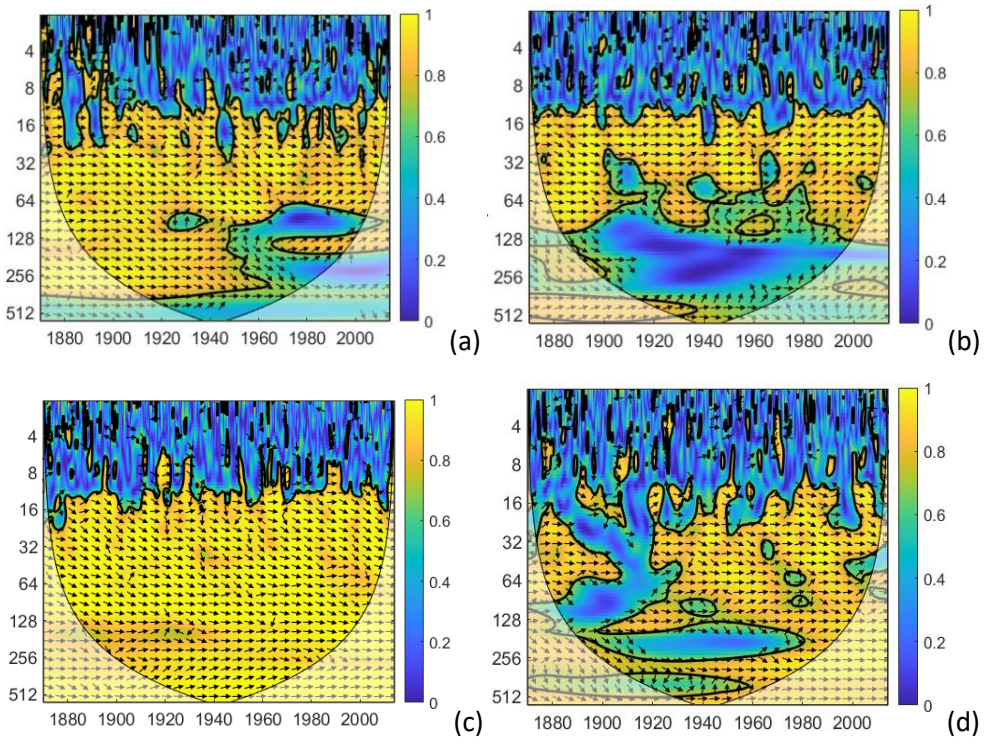

Fig. 1. Coherence of Nino3 and Nino4 anomalies for 1870–2020 by monthly data based on observations (a) and from simulations with historical scenario with 3 climate models: ACCESS-CM2 (b), CanESM5 (c) and INM-CM5-0 (d). Ordinates – periods in months, abscisses – time in years. Solid lines separate the regions of boundary effects, and bold lines limit the regions where coherence is nonzero at a significance level $p = 0.05$.

Changes in El Niño phenomena of various types according to empirical data after the middle of the 20th century differ significantly (Fig. 1a). This may not necessarily be due to real changes, but to the quality of earlier data [4]. The closest correspondence with Fig. 1a was obtained from simulations with the ACCESS-CM2 model (Fig. 1b). According to simulations with the CanESM5 model, a strong coherence of the Niño3 and Niño4 indices was obtained for all periods of more than a year for the entire analyzed time interval 1870–2020.

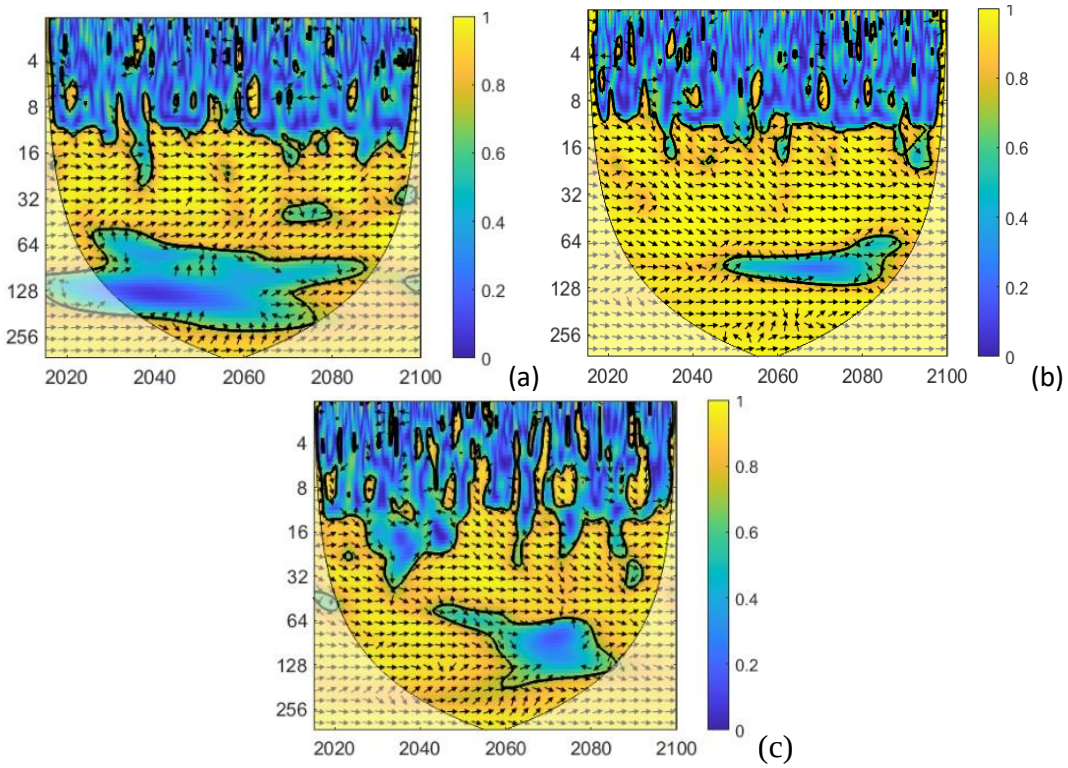

Fig. 2. Coherence of Nino3 and Nino4 anomalies from simulations for the 21st century with scenario SSP585 with 3 climate models: ACCESS-CM2 (a), CanESM5 (b) and INM-CM5-0 (c). Ordinates – periods in months, abscisses – time in years. Solid lines separate the regions of boundary effects, and bold lines limit the regions where coherence is nonzero at a significance level $p = 0.05$.

Figures 2(a-c) show coherence of Nino3 and Nino4 anomalies for 1870–2020 by monthly data from simulations for the 21st century under scenario SSP585 with climate models ACCESS-CM2, CanESM5 and INM-CM5-0. For ACCESS-CM2, with the best agreement with empirical data after 1950 (Fig.1b and Fig. 1a), with an overall high coherence of Niño3 and Niño4 for periods from one year to 5 years and more than 2 decades, their coherence does not appear for interdecadal variations until the last decade 21 century. All analyzed models show significant coherence for variations with periods about two decades and longer.

References

1. Kug J.S., Jin F.F., An S.I. Two types of El Nino events: Cold tongue El Nino and warm pool El Nino. *J. Cli.*, 2009, **22**, 1499–1515.
2. Jevrejeva S., Moore J., Grinsted A. Influence of the Arctic Oscillation and El Niño-Southern Oscillation (ENSO) on ice conditions in the Baltic Sea: The wavelet approach. *J. Geophys. Res.*, 2003, **108** (D21), 4677, doi:10.1029/2003JD003417.
3. Mokhov I.I. Changes in the frequency of phase transitions of different types of El NIno phenomena in recent decades. *Izv., Atmos. Oceanic Phys.*, 2022, **58** (1), 1-6.
4. Mokhov I.I., Medvedev N.N. The amplitude–frequency features of different El Nino types and their changes in recent decades. *Moscow Univ. Phys. Bull.*, 2022, 77 (3), 542-548.

Cold air outbreaks in the Barents Sea: dependence on sea-ice based on ECHAM6 model simulations

Alexandra Narizhnaya[1], Alexander Chernokulsky[1], Dörthe Handorf[2]

[1]*A.M. Obukhov Institute of Atmospheric Physics, Russian Academy of Sciences*

3 Pyzhevsky, 119017 Moscow, Russia

[2] *Alfred Wegener Institute, Helmholtz Centre for Polar and Marine, Potsdam, Germany*

Introduction

Changes in the heat and moisture fluxes between the ocean and the atmosphere have been observed in many regions due to global warming. In particular, in the Arctic region such changes are especially noticeable within the marine cold air outbreaks (MCAOs), i.e., events of the rapid advection of cold air from the ice-band regions to open-water areas. MCAOs in the Arctic play an important role in the energy exchange between the ocean and the atmosphere. In particular, the sensible and latent heat fluxes in MCAO amount to 200-500 W/m2. This results in the certain structure-development of convective clouds and its transformation within MCAO.

Previously, the variability of MCAOs in the seas of the Russian Arctic was estimated in (Narizhnaya et al., 2020). Trends as well as differences between the characteristics of MCAOs within the seas of the Western and the Eastern sector of the Russian Arctic were revealed. It was hypothesized that MCAOs changes can be associated with sea-ice decrease.

In this study, we evaluated results of numerical simulations with idealized boundary conditions to disentangle the role the role of sea ice concentration (SIC) in MCAOs characteristics changes in the Barents Sea (BS).

Data and methods

MCAOs were determined through the MCAO-index (Fletcher et al., 2016) calculated as a difference in vertical potential temperature between the surface and 800-hPa level. All MCAOs were classified according to their intensity as weak, moderate and strong.

We analyzed results of four sensitivity experiments with the atmospheric general circulation model ECHAM6 (Stevens et al., 2013) with different boundary conditions.

Corresponding author: Alexandra Narizhnaya, A.M. Obukhov Institute of Atmospheric Physics, Russian Academy of Sciences, Moscow, Russia.
E-mail: alex.narizhnaya@ifaran.ru

In the experiments (100 years each), different values of sea surface temperature (SST) and SIC were implemented into the model as boundary conditions, i.e., low and high SST (corresponding to SST for 1979-1983 and 2002-2006, respectively), low and high SIC (corresponding to SIC for 1979-1983 and 2005-2009, respectively) – see Fig. 1.

a

Boundary Conditions
Low SST (LSST) from 1979 to 1983
High SST (HSST) from 2002 to 2006
High ice (HICE) from 1979 to 1983
Low ice (LICE) from 2005 to 2009

b

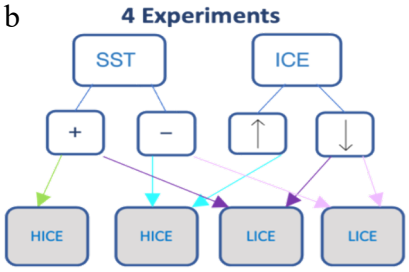

Fig.1. Table (a) and schematic representation (b) of model input boundary conditions for each of 4 model simulations.

Results

We found that over the BS model experiments show higher values of the MCAO-index associated with lower SIC, which implied their negative correlation. In particular, in the south of BS, values of the MCAO-index were up to 30% higher in the low-SIC experiments compared to the high-SIC experiments (Fig.2).

In particular, statistically significant changes are revealed for the months from January till April with differences in mean MCAO-index values up to 1.4. Changes of SST meanwhile do not significantly affect MCAOs characteristics.

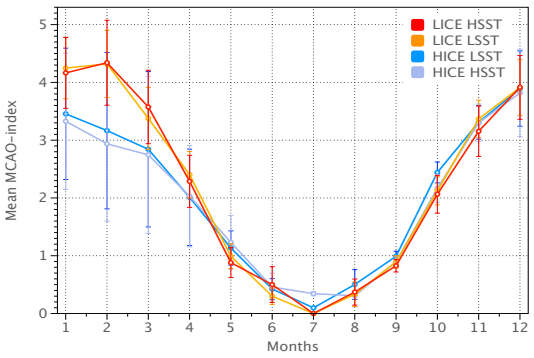

Fig. 2 Interannual variability of the MCAO-index averaged over the South Barents Sea region.

At the same time, the experiments with high SIC obtained lower mean values of the MCAO-index, but stronger interannual variability. Statistical differences (at the 95% level of significance) are evident between pairs with different SIC in the period from January to May (see Table 1). At the same time, statistically significant differences in experiments with the same SIC conditions but different SST were noted only for October.

	Jan	Feb	Mar	Apr	May	Jn	Jl	Aug	Sep	Oct	Nov	Dec
HICE LSST-HICE HSST	o	o	o	o	o	o	o	o	o	I	o	o
HICE LSST-LICE HSST	I	I	I	I	I	o	–	o	o	I	o	o
HICE LSST-LICE LSST	I	I	I	I	o	o	–	o	o	I	o	o
HICE HSST-LICE HSST	I	I	I	I	I	o	–	o	o	o	o	o
HICE HSST-LICE LSST	I	I	I	I	I	o	–	o	o	o	o	o
LICE HSST-LICE LSST	o	o	o	o	o	o	–	o	o	o	o	o

Table 1 Significance of difference (at the 95% significance level) between pairs of 4 experiments of the ECHAM6 model.

It is worth noticing that under LICE conditions MCAOs spread over much larger areas but with lesser mean MCAO-index values in comparison with HICE condition (see Fig. 3).

Previously, the variability of MCAOs in the seas of the Russian Arctic was assessed in (Narizhnaya et al., 2020). Based on reanalysis data, a marked decrease in MCAO intensity and

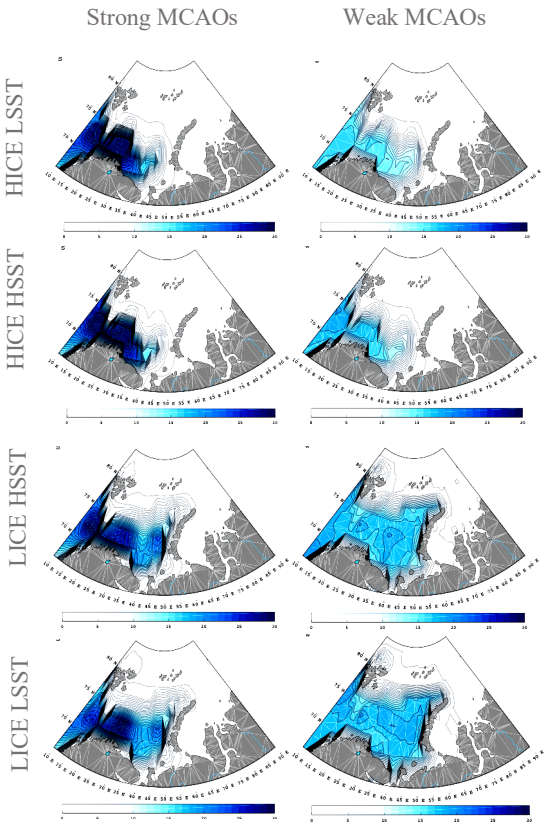

Fig.3 Frequency of occurrence (%) of strong and weak cold air outbreaks (left and right column, respectively) in the Barents Sea in January (1979-2018) according to 4 experiments of the ECHAM6 model.

SIC area was found, resulting in a positive relationship between SIC and MCAO-index over BS. That is in contrast to results of model experiments, obtained in the present study. This discrepancy between model simulation and reanalysis data should be investigated in further studies.

References

Fletcher J. K., Mason S., Jakob C. A climatology of clouds in marine cold air outbreaks in both hemispheres //Journal of Climate. – 2016. – Т. 29. – №. 18. – С. 6677-6692.

Narizhnaya A. I. et al. Marine cold air outbreaks in the Russian Arctic: climatology, interannual variability, dependence on sea-ice concentration //IOP Conference Series: Earth and Environmental Science. – IOP Publishing, 2020. – Т. 606. – №. 1. – С. 012039.

Stevens B. et al. Atmospheric component of the MPI-M Earth system model: ECHAM6 //Journal of Advances in Modeling Earth Systems. – 2013. – Т. 5. – №. 2. – С. 146-172.